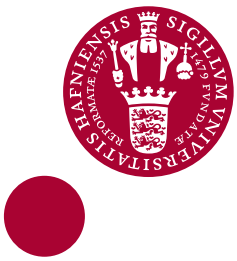

Integrative Characterization of the R6/2 Mouse Model of Huntington's Disease Reveals Dysfunctional Astrocyte Metabolism

Skotte, Niels H.; Andersen, Jens V.; Santos, Alberto; Aldana, Blanca I.; Willert, Cecilie W.; Nørremølle, Anne; Waagepetersen, Helle S.; Nielsen, Michael L.

Published in:
Cell Reports

DOI:
10.1016/j.celrep.2018.04.052

Publication date:
2018

Document version
Publisher's PDF, also known as Version of record

Resource

Cell Reports

Integrative Characterization of the R6/2 Mouse Model of Huntington's Disease Reveals Dysfunctional Astrocyte Metabolism

Graphical Abstract

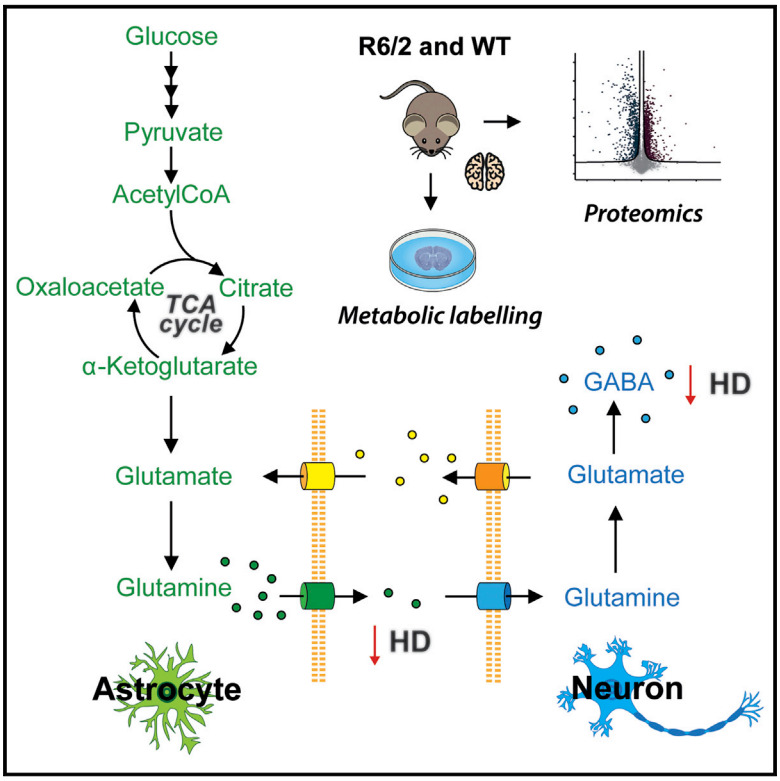

Highlights

- Spatial brain proteome in R6/2 mouse model is compromised at multiple pathways
- Impaired synapse energy metabolism and neurotransmitter homeostasis in R6/2 mice
- Decreased astrocytic glutamine release in R6/2 mice results in lower GABA labeling

Authors

Niels H. Skotte, Jens V. Andersen, Alberto Santos, ..., Anne Nørremølle, Helle S. Waagepetersen, Michael L. Nielsen

Correspondence

michael.lund.nielsen@cpr.ku.dk

In Brief

Skotte et al. report that systems-wide analysis of the R6/2 mouse spatial proteome identifies key protein changes related to energy metabolism, synapse function, and neurotransmitter homeostasis. Astrocytic glutamate-GABA-glutamine cycling is compromised, causing impaired glutamine release and, consequently, GABA synthesis. Thus, therapeutic strategies to improve astrocytic glutamine homeostasis may ameliorate symptoms in HD.

Data and Software Availability

PXD008099

Skotte et al., 2018, Cell Reports *23*, 2211–2224
May 15, 2018
https://doi.org/10.1016/j.celrep.2018.04.052

CellPress

Cell Reports
Resource

Integrative Characterization of the R6/2 Mouse Model of Huntington's Disease Reveals Dysfunctional Astrocyte Metabolism

Niels H. Skotte,[1,4] Jens V. Andersen,[2,4] Alberto Santos,[1] Blanca I. Aldana,[2] Cecilie W. Willert,[3] Anne Nørremølle,[3] Helle S. Waagepetersen,[2] and Michael L. Nielsen[1,5,*]

[1]Proteomics Program, The Novo Nordisk Foundation Centre for Protein Research, Faculty of Health Sciences, University of Copenhagen, 2200 Copenhagen, Denmark

[2]Department of Drug Design and Pharmacology, Faculty of Health and Medical Sciences, University of Copenhagen, Copenhagen, Denmark

[3]Department of Cellular and Molecular Medicine, Faculty of Health and Medical Sciences, University of Copenhagen, Copenhagen, Denmark

[4]These authors contributed equally

[5]Lead Contact

*Correspondence: michael.lund.nielsen@cpr.ku.dk

https://doi.org/10.1016/j.celrep.2018.04.052

SUMMARY

Huntington's disease is a fatal neurodegenerative disease, where dysfunction and loss of striatal and cortical neurons are central to the pathogenesis of the disease. Here, we integrated quantitative studies to investigate the underlying mechanisms behind HD pathology in a systems-wide manner. To this end, we used state-of-the-art mass spectrometry to establish a spatial brain proteome from late-stage R6/2 mice and compared this with wild-type littermates. We observed altered expression of proteins in pathways related to energy metabolism, synapse function, and neurotransmitter homeostasis. To support these findings, metabolic ^{13}C labeling studies confirmed a compromised astrocytic metabolism and regulation of glutamate-GABA-glutamine cycling, resulting in impaired release of glutamine and GABA synthesis. In recent years, increasing attention has been focused on the role of astrocytes in HD, and our data support that therapeutic strategies to improve astrocytic glutamine homeostasis may help ameliorate symptoms in HD.

INTRODUCTION

Huntington's disease (HD) is an autosomal dominant neurodegenerative disorder characterized by loss of voluntary motor control, psychiatric disturbances, and cognitive decline. The symptoms start in mid-life and are followed by a gradual decline, leading to death 15–20 years after the onset of symptoms (Ross and Tabrizi, 2011). The disease is caused by an expansion of the CAG repeat in the huntingtin (*HTT)* gene, causing an elongation of the polyglutamine tract in the ubiquitously expressed huntingtin protein (HTT) (Novak and Tabrizi, 2010). Despite the predictive ability to identify mutation carriers before disease onset, there is currently no therapy available that can delay the onset or slow disease progression of HD. However, after many years of preclinical development, promising results have been observed in the first human gene therapy trial to lower the toxic mutant HTT protein. The mutant HTT protein causes neuropathology with a reduction of the striatum and thinning of the cortex, starting more than a decade before the appearance of the symptoms (Aylward et al., 2011). In particular, neurons of the striatum and neurons that project from the cortex to the striatum are more susceptible to mutant HTT (Rosas et al., 2008; Aylward et al., 2012). The basis of the selective neuronal vulnerability in HD remains elusive but may in part be explained by defects in energy metabolism, especially since it has become evident that energetic malfunctions are present in the HD brain and may be a central mechanism in HD pathology (Browne and Beal, 2004; Kim et al., 2010; Mochel et al., 2012; Tang et al., 2013). This notion is not unique to HD, and the high demand of the cerebral metabolic machinery and impairments in brain energy and neurotransmitter metabolism have been linked to several neurological diseases (Attwell and Laughlin, 2001; Mergenthaler et al., 2013; Camandola and Mattson, 2017). In recent years, attention has shifted from a neuron-centric focus to the role of glial cells and especially astrocytes in HD (Acuña et al., 2013; Tong et al., 2014; Benraiss et al., 2016; Khakh et al., 2017). In the brain, astrocytes are the most abundant cell type and are tightly associated with the synapse, where they are responsible for modulating synaptic transmission as well as providing metabolic support to the neurons (Bélanger et al., 2011). Astrocytes play a crucial role in up-take of the neurotransmitter glutamate and providing neurons with glutamine, an important precursor for glutamate and gamma-aminobutyric acid (GABA) synthesis (called the glutamate-GABA-glutamine cycle) (Sonnewald et al., 1993; Bak et al., 2006b).

To get a better understanding of the molecular pathogenesis of HD, we first performed a systems-wide exploration of protein changes in four brain regions (striatum, cortex, hippocampus, and midbrain) from 12-week-old transgenic R6/2 mice. Notably, R6/2 mice recapitulate several HD phenotypes, including movement disturbances, muscle wasting, and premature death at about 14 to 16 weeks (Mangiarini et al., 1996), and, therefore, constitute a commonly used HD model system (Menalled and Brunner, 2014). To this end, we applied an unbiased and

systems-wide proteomics strategy recently described for determination of quantitative brain analyses (Sharma et al., 2015). Using this strategy, we identified 6,801 proteins and quantified their expression changes across the different brain regions. Reassuringly, we observed the most aberrant expression changes in the striatum and cortex. Among the differentially regulated proteins, we found significant enrichment of proteins belonging to several pathways relevant for glutamate signaling, synapse function, and neurotransmitter homeostasis. Moreover, several protein changes in key metabolic pathways, including glycolysis, the tricarboxylic acid (TCA) cycle, and the glutamate-GABA-glutamine cycle, were observed. Our findings are supported by a recent temporal study where proteomic analyses demonstrated that a large number of proteins with potential links to HD accumulate in aggregates (Hosp et al., 2017), including some of the key candidates identified in this study. Based on our findings, we conducted functional metabolic analyses on acutely isolated brain slices from the striatum and cortex using stable ^{13}C-labeled energy substrates coupled to gas chromatography-mass spectrometry (GC-MS) analyses. The metabolic experiments supported our proteomics findings and demonstrated that astrocytic metabolism and neurotransmitter dynamics are impaired whereas neuronal metabolism seems largely unaffected under our conditions.

RESULTS

Spatial Brain Proteome in the R6/2 Mouse

To map the spatial brain proteome, we microdissected the brains of four wild-type (WT) and R6/2 mice into four central regions (striatum, cortex, hippocampus, and midbrain) and subsequently profiled protein expression changes by MS analysis (Figure 1A; Table S1). To establish a baseline for the technical and biological quality, we first evaluated the WT proteome separately (Figure S1A). We found a strong correlation between replicates (Pearson correlation ranging from 0.97–0.99) (Figure S1B), and the high reproducibility in our analysis was further supported by a principal-component analysis (PCA) detailing a clear separation of the four different brain regions (Figures S1C and S1D). To assess the biological background, we next performed a multiple comparisons analysis test to identify significant protein changes across the four brain regions (Figure S1E; Table S2). Collectively, the expression profiles from the striatum, cortex, and hippocampus clustered well together compared with the midbrain, with gene ontology (GO) enrichment and pathway analyses revealing 9 clusters to be enriched across the individual brain regions (Table S2; Figure S1E). Collectively, these results are comparable with previous observations from a deep brain proteome study (Sharma et al., 2015) and confirm the reliability of our analytical strategy.

Having established the spatial brain proteome for WT mice, we next investigated the brain proteome from 12-week-old R6/2 mice with 190–200 CAG repeats (Reynolds et al., 2017) in a similar manner. These mice display progressive clasping starting at 8 weeks of age, with a complete clasping phenotype at 11 weeks of age (Figure S2), similar to previous observations for the R6/2 mouse with 160 CAG repeats (Cummings et al., 2012). In total, we identified 6,801 proteins, and 5,555 were selected for further investigations (Figure 1B; Table S1), with most of these proteins being comparable with proteins found in a recent temporal proteome study of the R6/2 mouse carrying a 150-CAG repeat expansion (Hosp et al., 2017). The majority of the selected proteins in our study were shared between all four brain regions across the two genotypes (Figure S1F), and, similar to the data obtained from WT mice, we observed strong reproducibility (Pearson correlations ranging from 0.96–0.99) between biological replicates (Figure 1C). Moreover, a three-dimensional PCA visualization showed a clear separation of brain regions and genotype (Figure 1D; Figures S1G and S1H), supporting that our proteomic analysis provides a sound basis for genotypic comparison.

Having established good reproducibility in our experimental setup and having validated that a quantitative comparison of spatial proteomes between WT and R6/2 brains is well founded, we next performed a systems-wide comparison of all brain regions and genotypes. Upon hierarchical clustering of HD and WT data, we observed that biological replicates, individual brain regions, and genotypes clustered strongly together (Figure 1E; Table S2). Several of the regulated protein clusters were enriched for terms previously associated with HD, including the glutamate signaling pathway ($p = 1.04 \times 10^{-7}$), protein oligomerization ($p = 1.03 \times 10^{-5}$), and the proteasome ($p = 1.02 \times 10^{-20}$) (Zuccato et al., 2010; Bates et al., 2015), whereas processes previously only gaining little attention included extracellular vesicular exosome ($p = 8.87 \times 10^{-7}$), divalent metal ion transport ($p = 2.05 \times 10^{-7}$), and metabolism of amino acids and derivatives ($p = 1.59 \times 10^{-12}$) (Figure 1F). Because of the spatial HD signature, we decided to investigate the individual brain regions in more detail (Figure 2A; Table S3). Across the four brain regions, we identified several protein changes, with a total of 750 and 764 proteins exhibiting increased or decreased expression, respectively, in R6/2 mice compared with the WT (Figure 2B). More specifically, the individual brain regions striatum, cortex, hippocampus, and midbrain exhibited 905, 779, 385, and 114 protein changes, respectively, which clearly reflects the vulnerability of the brain regions to the presence of mutant HTT (striatum > cortex >> hippocampus >>> midbrain). Moreover, the observed proteome changes are comparable with the number of differentially expressed genes in two R6/2 mouse models with 150 and 300 CAG repeats, respectively (Tang et al., 2011).

Among the regulated proteins (false discovery rate [FDR] > 0.05), we observed several candidates previously associated with HD (Zuccato et al., 2010; Bates et al., 2015). For example, we found a marked reduction in phosphodiesterase 10A (PDE10A) expression in the striatum and cortex, which is central for neuronal survival and an early marker of disease progression (Wilson et al., 2016). Similarly, we found a reduction in dopamine- and cyclic AMP (cAMP)-regulated phosphoprotein 32 kDa (DARPP-32) in the striatum and cortex, which is often used as a marker of medium spiny neuron (MSN) atrophy and neurodegeneration (Guo et al., 2012). Microtubule-associated protein tau (MAPT) expression was increased in the striatum and cortex, which is intriguing considering MAPT levels in cerebrospinal fluid, and has been suggested as a potential biomarker able to predict clinical phenotype in HD patients (Rodrigues et al., 2016). In addition, HAP1 (huntingtin-associated protein 1),

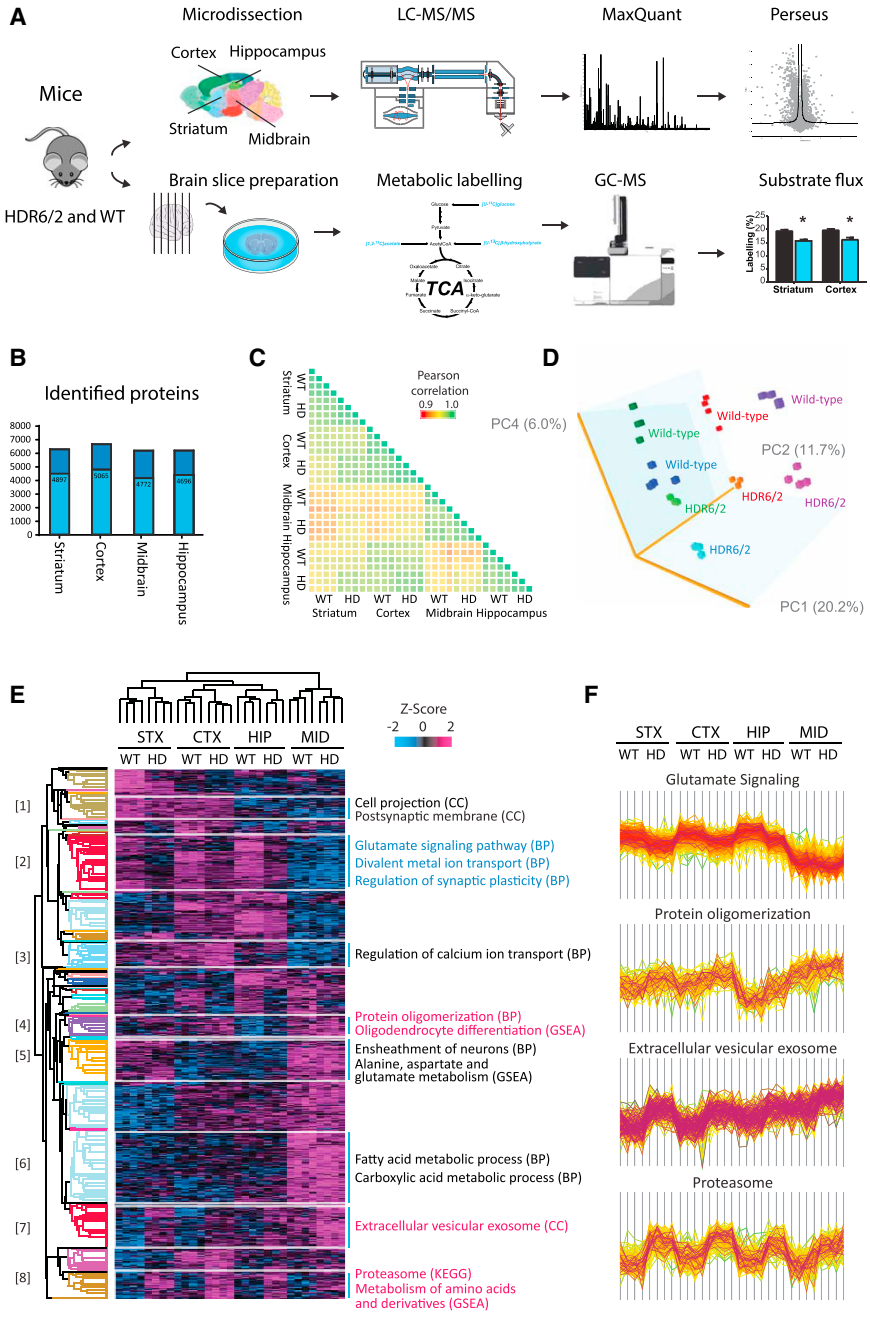

Figure 1. Spatial Protein Expression

(A) Brains from 12-week-old R6/2 mice were collected and micro-dissected into 4 brain regions (striatum, cortex, hippocampus, and midbrain) and subjected to LC-MS analysis with subsequent data analysis using MaxQuant and Perseus software. In addition, brain slices were isolated from the striatum and cortex, respectively, and used for metabolic ^{13}C labeling and subjected to GC-MS.

(B) The total number of identified proteins before and after filtering (3 of 4).

(C) Diagram displaying the Pearson correlation between the individual samples from the 4 regions and the 2 genotypes.

(D) PCA (principal-component analysis) demonstrating the difference of the 4 different regions and 2 genotypes using three PCs (principal components): PC1, PC2, and PC4.

(E) Cluster analysis demonstrating the grouping of the replicate samples and 8 clusters with significantly enriched pathways related to brain region and genotype of a total of 13 clusters.

(F) Expression levels are illustrated for 4 selected clusters, including glutamate signaling (10 genes, Benjamini-Hochberg p = 1.04E−03), protein oligomerization (13 genes, Benjamini-Hochberg p = 3.59E−02), proteasome (18 genes, Benjamini-Hochberg p = 1.97E−16), and extracellular vesicular exosome (90 genes, Benjamini-Hochberg p = 1.11E−03), and both genotypic and tissue-specific differences can be observed. Proteins belonging to the selected annotation are shown in purple, and proteins belonging to the cluster are shown in yellow to green based on distance from the mean of all proteins in the cluster.

which participates in intracellular vesicle transport (Wu and Zhou, 2009), showed increased expression across all regions except the midbrain. Moreover, three proteins from the Serpine superfamily (SERPIN A3M, -A3K, and -A1E), which are murine paralogs to the human α1-antichymotrypsin and α1-antitrypsin, were decreased in all brain regions, consistent with a previous study showing decreased α 1-antitrypsin in R6/2 and human HD brains (Zabel et al., 2002). Collectively, our findings demonstrate several similarities at the molecular level between R6/2 mice and HD patients and support the strong foundation of our study.

Next we performed a pathway enrichment analysis (Table S3). To encapsulate the commonalities of the changed processes across the brain regions, we condensed the data and visualized the GO terms for cellular components (GOCCs) and biological processes (GOBPs) as individual networks (Figures 2C and 2D; Table S4; Figures S2 and S3). The majority of the terms were strongly associated with synapse structure, function, and transmission, which illustrates the essential role of the synapse in the pathogenesis of HD. Importantly, synapse function is tightly coupled to energy metabolism as the restoration of ion gradients after action potentials as well as uptake and recycling of neurotransmitters are some of the main processes contributing to the high energy demand of the brain (Harris et al., 2012). In support of this notion, we observed several dysregulated proteins in the R6/2 mouse related to energy metabolism, including glycolysis, the TCA cycle, and the glutamate-GABA-glutamine cycle (Figure 3). This list of proteins included several key proteins predominantly confined to astrocytes, including the glutamate transporter excitatory amino acid transporter 2 (EAAT2) (Bak et al., 2006b; Bélanger et al.,

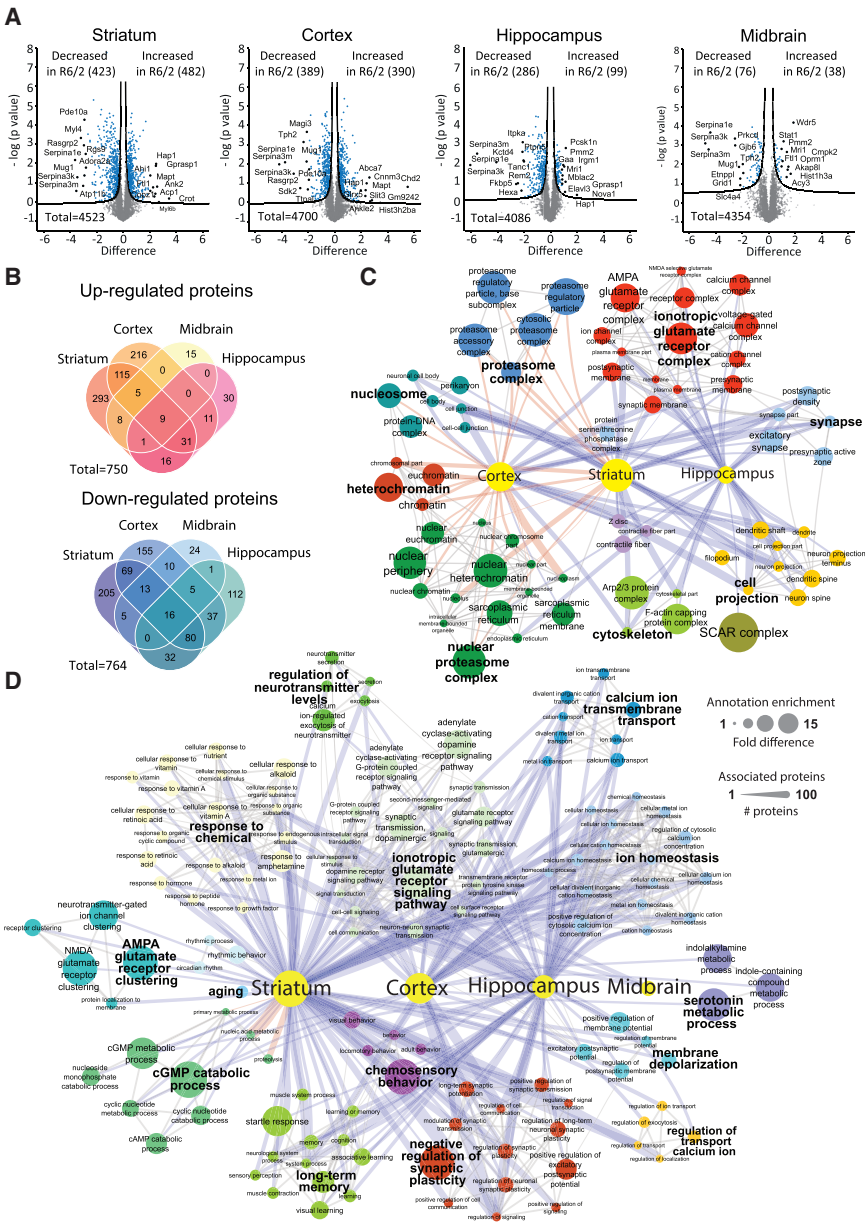

Figure 2. Protein Changes in Huntington's Disease

(A) Volcano plots illustrate the significant protein expression changes. The top 10 proteins with the highest or lowest fold difference are marked on the blot for all 4 brain regions (FDR > 0.05).

(B) 764 and 750 proteins show decreased and increased expression in HD tissues, respectively. Shown is the number of enriched pathways across the 4 regions based on proteins with either increased (orange) or decreased (blue) expression.

(C and D) Networks built on enriched GOCC terms (C) and GOBP terms (D) for a representative visualization of the changes in the HD brain. All 11 identified clusters are shown for GOCC, whereas the selected terms are shown for GOBP (Figures S3 and S4). Yellow nodes represent the different brain regions, and the size of the node illustrates the number of changed proteins for each region. The remaining colored nodes represent the individual enriched terms, and the size of the node marks the enrichment factor for that specific annotation term (Table S4). The lines illustrate the number of associated proteins for each annotation term. Blue lines represent proteins with decreased expression in HD compared with the WT, whereas red lines represent proteins with increased expression. The thickness of the lines illustrates the number of proteins connecting the brain regions to the annotation term.

Energy and Neurotransmitter Metabolism in R6/2 Mice

To establish a baseline for our metabolic brain slice experiments, we first measured a panel of amino acids using high-performance liquid chromatography (HPLC) in extracts of freshly prepared cortical and striatal slices from 12-week-old R6/2 and WT mice (Andersen et al., 2017b). Overall, we found that glutamine levels were significantly elevated in cortical slices ($p = 0.048$), with a similar tendency present in striatal slices ($p = 0.124$) from R6/2 mice compared with the WT (Table S5). Likewise, we observed increased taurine levels in striatal ($p = 0.021$) and cortical ($p = 0.019$) slices from R6/2 mice. This observation is in line with previous studies establishing that elevated levels of taurine and glutamine are robust indictors of disease progression in both the striatum and cortex of R6/2 mice (Behrens et al., 2002; Tkac et al., 2007; Zacharoff et al., 2012).

To study energy metabolism in the isolated brain slices and to provide detailed insights into relevant metabolic pathways, we next used ^{13}C-labeled energy substrates and GC-MS analysis to quantify ^{13}C incorporation in central cellular metabolites (Andersen et al., 2017a). To this end, we incubated the slices at 37°C for 60 min with ^{13}C-labeled glucose and β-hydroxybutyrate (βHB) (McNair et al., 2017), which are metabolized to a greater

2011), glutamine synthetase (GS) (Walls et al., 2015), and the glutamine transporter sodium-coupled neutral amino acid transporter 3 (SNAT3) (Leke and Schousboe, 2016; Todd et al., 2017). Collectively, the observed expression changes pointed toward impaired astrocytic metabolism and function. However, since differentially regulated proteins and enzymes may still retain their function and catalytic activity, we decided to investigate the energy and neurotransmitter metabolism in acutely isolated brain slices to better understand the functional consequences of the observed protein dysregulation. Here, we applied brain slices from the two most affected regions (striatum and cortex) to obtain functional *ex vivo* ^{13}C labeling data using substrates that could distinguish between the astrocytic and neuronal compartments.

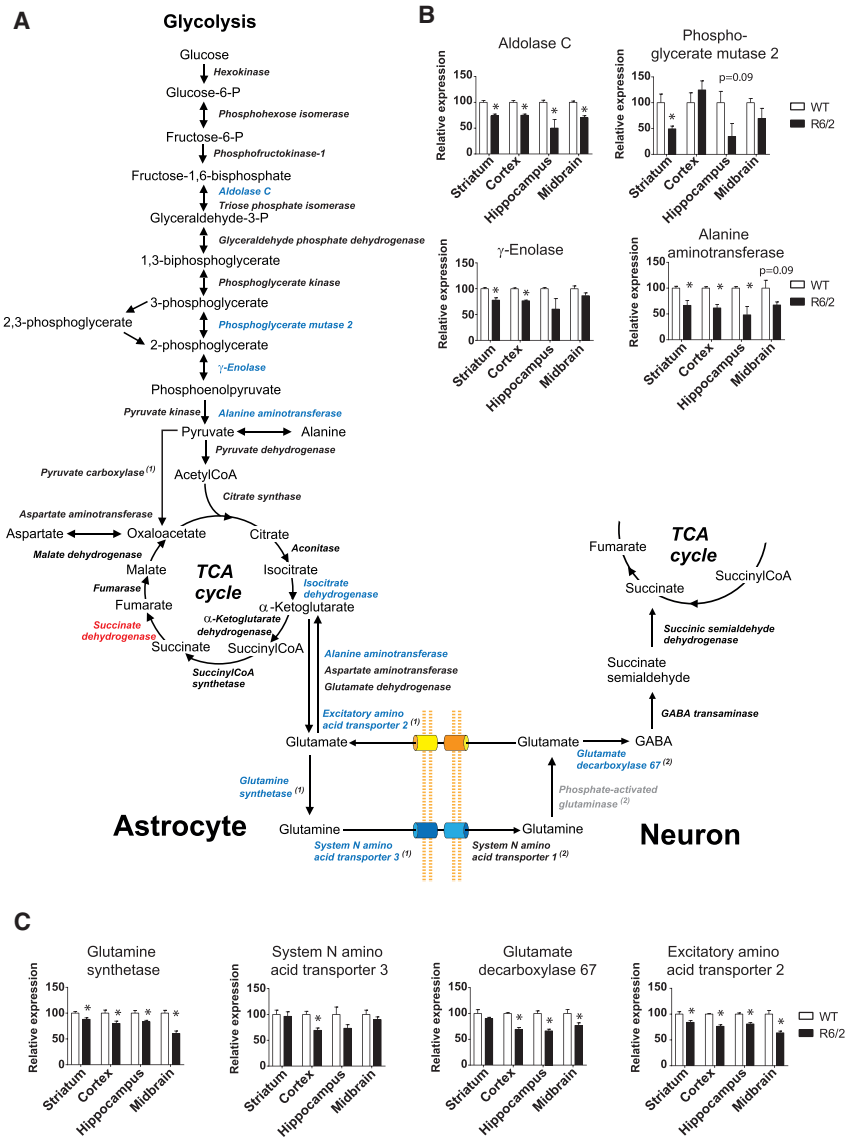

Figure 3. Energy Metabolism in Huntington's Disease

(A) Three central pathways for cerebral metabolism are illustrated with the associated key enzymes marked at each step. Glycolysis and the TCA cycle take place in both astrocytes and neurons but are only illustrated on the left (astrocyte) for simplicity. Substrates are marked in bold, and enzymes and transporter proteins are marked in italic font. Proteins with decreased expression in HD compared with the WT are marked in blue, whereas proteins with increased expression are marked in red. Proteins marked in gray were not quantified in our study. Proteins with preferential or confined expression to either astrocytes or neurons are marked with 1 or 2, respectively.

(B and C) The results for the glycolytic enzymes (B) and proteins involved in glutamate-glutamine-GABA cycling (C) are graphed for comparison across the different brain regions.

Data are represented as mean ± SEM. Significance with $p \leq 0.05$ is marked by an asterisk (n = 4 for each group).

extent in neurons compared with glial cells and, therefore, primarily reflect neuronal metabolism (Bak et al., 2006a; Achanta et al., 2017; Díaz-García et al., 2017). In our metabolic analysis, we observed minor changes in ^{13}C labeling of striatal and cortical slices incubated with either [U-^{13}C]βHB (Figure 4, blue bars) or [U-^{13}C]glucose (Figure S4, blue bars; Table S6). From the measured metabolism of [U-^{13}C]βHB, a slight decrease in glutamate ^{13}C labeling was observed in both the striatum ($p = 0.0026$) and cortex ($p = 0.0049$), along with decreased glutamine ^{13}C labeling in the striatum ($p = 0.0425$). The slight reduction in glutamate labeling was also observed from the metabolism of [U-^{13}C]glucose in striatal ($p = 0.030$) and cortical slices ($p = 0.0492$) of R6/2 mice. Collectively, these results indicate that the neuronal metabolism of glucose and βHB is largely preserved in R6/2 mice despite the reduced expression of glycolytic enzymes (Figure 3B). In contrast, when we used [1,2-^{13}C]acetate, which is metabolized preferentially in astrocytes and can be used as a metabolic marker of this compartment (Badar-Goffer et al., 1990; Sonnewald et al., 1993), we observed large reductions in ^{13}C labeling of α-ketoglutarate ($p = 0.0023$), aspartate ($p = 0.0030$), and glutamate ($p = 0.0151$) in striatal slices from R6/2 mice (Figure 4, green bars; Table S6). The decreased ^{13}C labeling in glutamate is likely linked to hampered astrocytic TCA cycle metabolism, as characterized by lower ^{13}C labeling in aspartate and α-ketoglutarate from [1,2-^{13}C]acetate metabolism. A similar trend was observed for cortical slices but did not reach statistical significance, whereas significant reductions in ^{13}C labeling of glutamine and GABA were observed in both the striatum ($p = 5.52 \times 10^{-4}$ and 5.19×10^{-7}, respectively) and cortex ($p = 0.0043$ and 0.0071, respectively). Considering that glutamine is exclusively synthesized in astrocytes and the main precursor for GABA synthesis in neurons (Sonnewald et al., 1993; Andersen et al., 2017b), our results indicate that limited amounts of glutamine reach the neuronal compartment. This reduction may stem from a lower availability of glutamate for glutamine synthesis, impaired synthesis of glutamine, reduced transfer of glutamine from the astrocyte to the neuron, or a permutation of them all. Interestingly, all three mechanisms are individually supported by our spatial proteome analysis, where we found a reduction in the expression of both the glutamate transporter EAAT2, the glutamine synthetase GS, and the glutamine transporter SNAT3 (Figure 3C).

To further investigate the compromised astrocytic energy metabolism, we next sought to specifically map the metabolism

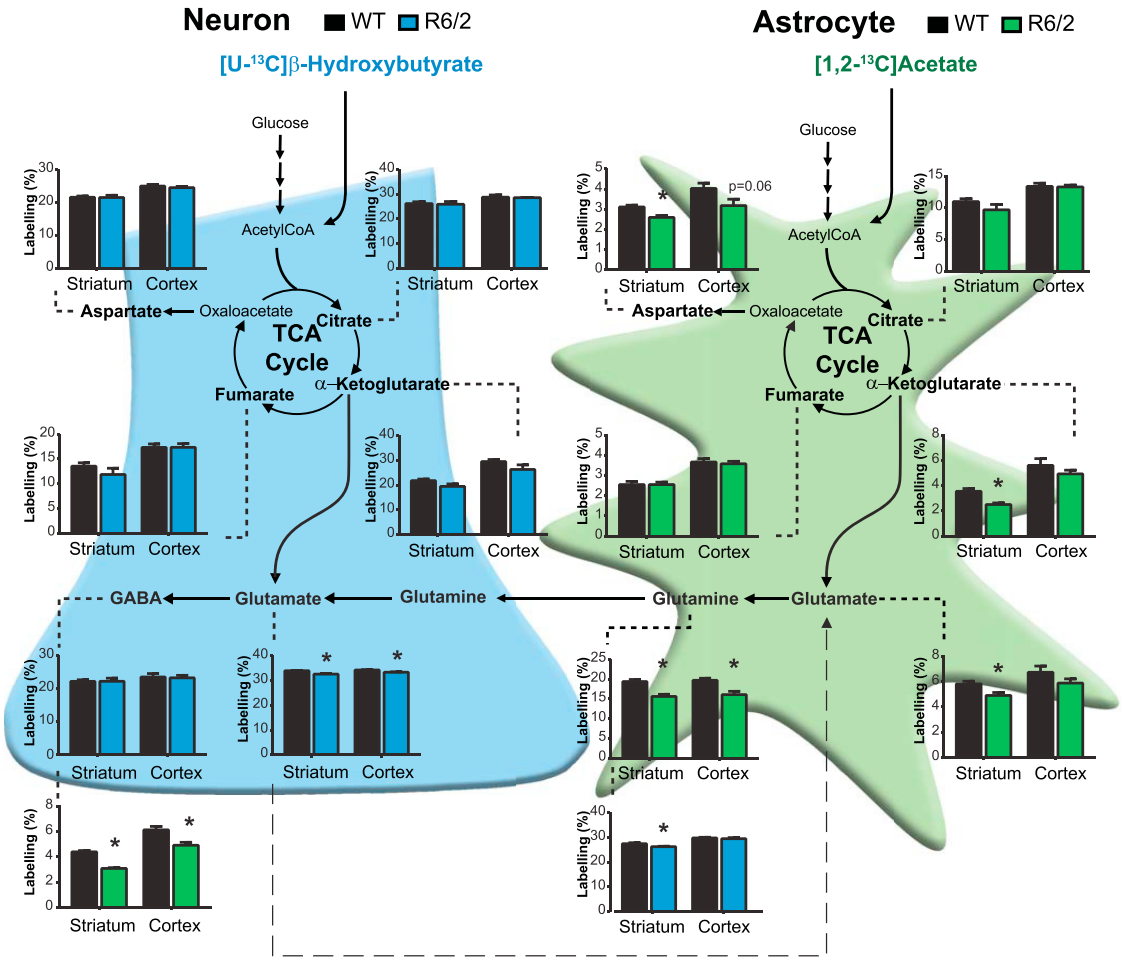

Figure 4. Metabolism of β-Hydroxybutyrate and Acetate

Brains slices were prepared from the striatum and cortex of 12-week-old R6/2 and WT mice and incubated in medium containing [U-^{13}C]β-hydroxybutyrate (βHB) (blue columns) and [1,2-^{13}C]acetate (green columns). βHB is metabolized predominantly in neurons, whereas acetate is preferentially metabolized in astrocytes. Hence, these substrates can be used as metabolic markers of these two compartments. ^{13}C incorporation was measured with GC-MS. Data are represented as mean ± SEM. *p ≤ 0.05 (n = 6 for each group). Additional information for GC-MS can be found in Table S6.

of glutamate and glutamine, which are key constituents of both neurotransmission and cerebral amino acid homeostasis (Albrecht et al., 2010; Walls et al., 2015). Released neurotransmitter glutamate is primarily removed from the synapse by adjacent astrocytes (Bélanger et al., 2011). In the astrocytes, glutamate can be converted into glutamine or used for other purposes, including cellular energy metabolism. Glutamine synthesized in the astrocyte is transported to neurons and converted into glutamate for oxidative metabolism or neurotransmission (Figure 3). Overall, we observed no changes in the metabolism of glutamine (Figure 5, orange bars; Figure S6), whereas uptake of [U-^{13}C]glutamate was slightly decreased in cortical slices ($p = 0.0133$) from R6/2 mice (Figure 5, red bars; Figure S6), which agrees with reduced expression of the glutamate transporter EAAT2. In addition, striatal reductions in ^{13}C labeling of the TCA cycle intermediates α-ketoglutarate ($p = 0.0462$), fumarate ($p = 0.0319$), and citrate ($p = 0.0106$) were observed, and reduced ^{13}C labeling of aspartate was found in both striatal ($p = 0.0050$) and cortical slices ($p = 0.0423$) from R6/2 mice compared with the WT. As observed for incubation with [1,2-^{13}C]acetate, ^{13}C labeling of GABA from the metabolism of [U-^{13}C]glutamate was significantly reduced in both the striatum ($p = 0.0052$) and cortex ($p = 0.0166$), indicating that malfunctions in the astrocytic compartment affect the synthesis of this central inhibitory neurotransmitter. This notion is supported by elevated absolute levels of glutamine after incubation with [U-^{13}C]glutamate (Table S5), indicating sufficient glutamine synthesis, whereas impaired release of glutamine from astrocytes likely leads to its accumulation, hampering neuronal GABA synthesis.

DISCUSSION

Here, we describe an integrative analysis of regulated differences in the proteome and metabolic and neurotransmitter intermediates in the brain of R6/2 mice compared with WT littermates. Our proteome analysis demonstrated that key proteins

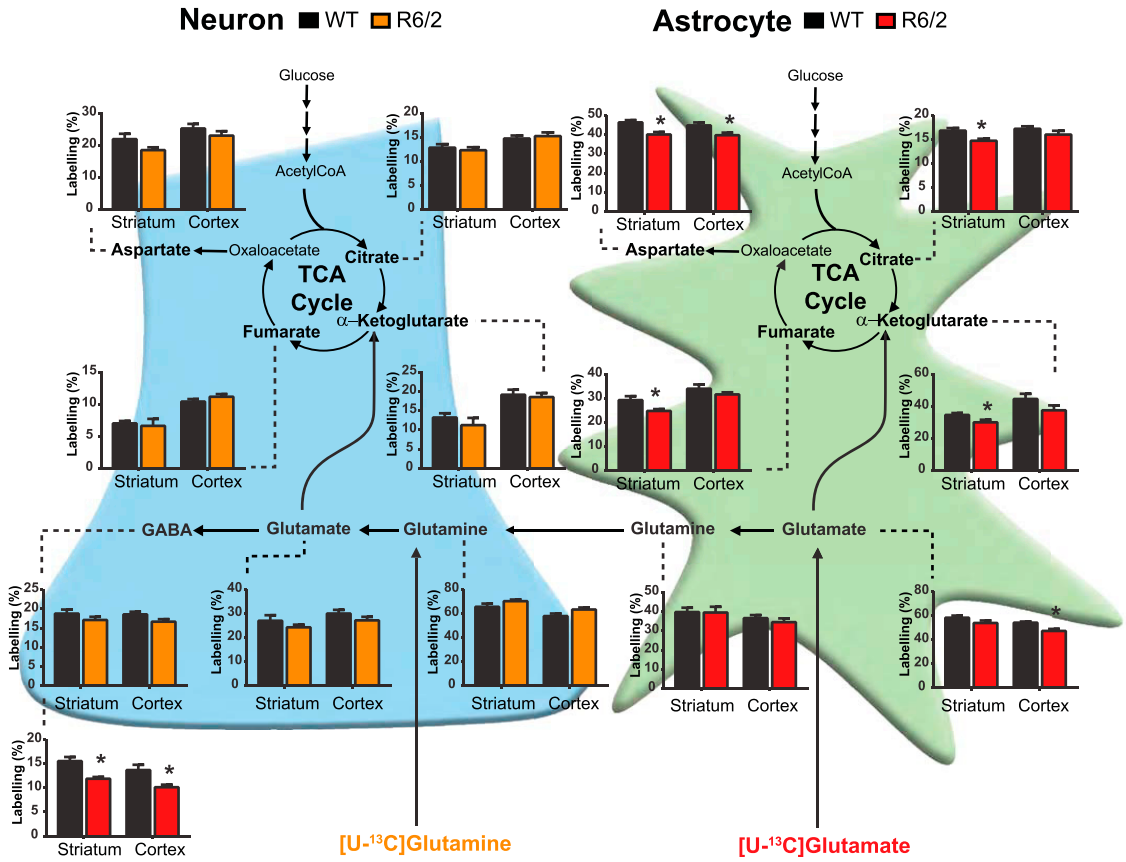

Figure 5. Metabolism of Glutamate and Glutamine

Brains slices were prepared from the striatum and cortex of 12-week-old R6/2 and WT mice and incubated in medium containing [U-^{13}C]glutamine (orange columns) and [U-^{13}C]glutamate (red columns). Glutamine is metabolized predominantly in neurons, whereas glutamate is preferentially taken up and metabolized in astrocytes. Hence, these substrates can be used as metabolic markers of these two compartments. ^{13}C incorporation was measured with GC-MS. Data are represented as mean ± SEM. *$p \leq 0.05$ (n = 6 for each group). Additional information for GC-MS can be found in Table S6.

involved in synapse function and energy metabolism are dysregulated, which led us to further investigate the consequences of these changes at the level of energy metabolism and amino acid homeostasis. To this end, we used *ex vivo* brain slices that demonstrated impaired glial metabolism, resulting in hampered neuronal GABA synthesis, likely as a consequence of reduced glutamine release by astrocytes.

We used state-of-the-art MS technology to investigate molecular changes in the R6/2 HD mouse model with 190–200 CAG repeats at the age of 12 weeks (Reynolds et al., 2017), which corresponds to the late stages of the disease. These mice demonstrate a similar progression in behavior as mice with 150 CAG repeats (Cummings et al., 2012; Figure S1) and a similar severity of molecular changes (Tang et al., 2011). Furthermore, we found elevated cerebral levels of taurine (Table S5), which has previously been demonstrated to be a robust marker of disease progression, in the R6/2 mouse, manifesting around 8–9 weeks of age (Behrens et al., 2002; Tsang et al., 2006; Zacharoff et al., 2012).

Previously, MS-based studies have been conducted to map protein expression changes across several different HD models, including R6/2 (Perluigi et al., 2005; Liu et al., 2007; Zabel et al., 2009; Hosp et al., 2017), Q92 and Q150 (Deschepper et al., 2012), and YAC128 (Wegrzynowicz et al., 2012) mice as well as an HD rat model (Cong et al., 2012). Although these studies reported interesting and supportive observations, they did not focus on the metabolic aspects of astrocytes described here. Furthermore, we included analysis of the midbrain region in our study, not previously investigated by proteomics, and thereby provide an additional resource to the research community.

Initially, we validated our experimental approach by demonstrating a strong technical and biological reproducibility across brain regions, which allowed a clear separation of regions and genotypes (Figures 2C and 2D). Reassuringly, the data demonstrated that the striatum is the most affected region at the proteome level, whereas the midbrain entails the least expression differences (Figure 2A), which is in line with general HD pathology (Waldvogel et al., 2015). This was also supported by our metabolic studies, where metabolism of the striatal slices was more affected compared with cortical slices in the R6/2 mice. In the striatum, we found, in total, 905 proteins with altered expression in R6/2 compared with WT mice, which supports that the analyzed mice were in the late stages of the disease. The scale of molecular changes is supported by a gene profiling study in the R6/2 mouse with 150 CAG repeats (Tang et al., 2011), where

997 differentially regulated genes were observed in the striatum from 12-week-old mice. Importantly, when we compared the identified proteins with previous HD studies, we reassuringly found that several of the dysregulated proteins (Figure 2A; Table 1) have been associated with HD, including PDE10A, DARPP-32, HAP1, MAPT, and SERPIN-A1E (Zuccato et al., 2010; Bates et al., 2015), serving as strong corroboration of our proteome study. Moreover, the top 20 protein candidates from a recent proteome study in R6/2 mice with 150 CAG repeats, which were selected based on their similarity to the expression profile of PDE10A, were all confirmed in our dataset and served as a solid validation of the two independent studies (Hosp et al., 2017).

Overall, proteins with decreased expression were mostly related to biological processes such as synapse function and neurotransmitter homeostasis, whereas proteins with increased expression belonged to a few processes, including chromatin regulation and the proteasomal machinery (Figures 2D and 2E; Table S4). From our detailed analysis of proteins involved in energy metabolism and amino acid homeostasis, we observed several changes in key proteins involved in glycolysis, the TCA cycle, and glutamate-GABA-glutamine cycling (Figure 3). To corroborate our findings, we investigated the temporal expression profiles of key proteins using recently published proteome data (Hosp et al., 2017). Here, we found an overall strong correlation between the two datasets (Figure 3; Figure S5) and observed that the glycolytic enzymes aldolase C (ALDOC), phosphoglycerate mutase 2 (PGAM2), and gamma-enolase (ENO2) were already reduced at the age of 8 weeks, demonstrating that the changes observed in our study occur earlier in the disease progression. Similar results can be seen for the proteins involved in glutamate-GABA-glutamine cycling, including EAAT2, SNAT3, and GS, which also appear to be reduced already at 8 weeks (Figure S5). Hosp et al. (2017) also observed a temporal trend toward a reduction in glutamate decarboxylase 67 (GAD67); however, their quantitative data did not reach statistical significance. Still, other studies support our findings of diminished GAD67 expression by demonstrating reduced mRNA levels of GAD67 in both cultured neurons derived from induced pluripotent stem cells from HD patients (Lim et al., 2017) as well as in the striatum from 12-week-old R6/2 mice (Tang et al., 2011). Collectively, these results of early alterations in metabolic protein expression may suggest that metabolic deficits could be causal and not merely consequences of late-stage disease progression.

Even though the expression of multiple glycolytic enzymes was found to be downregulated (Figure 3), the regulation did not entail functional consequences because no changes were observed from metabolism of [U-^{13}C]glucose (Figure S4). This could indicate compensatory elevations in glycolytic activity despite reduced enzyme expression. This notion is supported by other studies in HD models, where activity or function are affected because of altered protein location or changes in post-translational modification (Perluigi et al., 2005; Huang et al., 2010; Skotte et al., 2017). For the TCA cycle, we found increased expression of two subunits in the cortex of the R6/2 mice (flavoprotein and cytochrome b) belonging to succinate dehydrogenase (SDH), also known as complex II of the electron transport chain. This is consistent with recent findings from both HD patients and Q175 HD mice, where SDN activity was found to be elevated in the cortex (Naseri et al., 2015). However, other studies in both mice and humans have also associated reductions in SDH with striatal vulnerabilities in HD (Beal et al., 1993; Brouillet et al., 1995; Benchoua et al., 2006). As an example, systemic injections with 3-nitroproprionic acid (3-NP), an SDH inhibitor, results in striatal degeneration mimicking HD pathology (Beal et al., 1993). The reason for this discrepancy remains unclear but could be related to the nature of the R6/2 mouse model since fluctuations in the expression pattern of SDH have been observed previously, where SDH was reduced at 2 weeks, increased at 4 weeks, and was again reduced at 8 weeks (Zabel et al., 2009).

At baseline, we found increased levels of glutamine and taurine in freshly prepared brain slices from R6/2 mice (Table S5). The basis for the increased taurine level is still unclear, but it may very well be a response to changes in osmolarity due to cellular aggregation of mutant HTT protein (Foos and Wu, 2002). Taurine has several functions in the brain, including neuromodulatory and osmolytic effects (Foos and Wu, 2002; Menzie et al., 2014). Taurine is also a weak GABA receptor agonist and can reduce glutamate-induced excitotoxicity (Albrecht and Schousboe, 2005), which has been suggested to play a central role in neurodegeneration associated with HD (Behrens et al., 2002; Foos and Wu, 2002; Menzie et al., 2014). Interestingly, taurine treatment of the 3-NP model described above improved certain behavior phenotypes as well as increased the level of GABA (Tadros et al., 2005). In contrast to taurine, where the mechanism behind its increase remains to be elucidated, we propose that the increase in glutamine may be a consequence of impaired glutamine release from astrocytes (Table S5), which is essential for synaptic replenishment of both glutamate and GABA.

Similar to our study, previous reports have shown decreased expression of the astrocytic glutamate transporters EAAT1 and EAAT2 (Behrens et al., 2002; Estrada-Sánchez et al., 2009; Tong et al., 2014; Dvorzhak et al., 2016), which led to the notion that elevated glutamate and over-activation of neuronal glutamate receptors would result in enhanced neuronal susceptibility to excitotoxic cell death (Behrens et al., 2002; Browne and Beal, 2004; Estrada-Sánchez et al., 2009; Tong et al., 2014; Dvorzhak et al., 2016). As a result of these studies, augmentation of glutamate uptake has been suggested as a viable therapeutic approach for HD. However, it has recently been shown that a brain slice preparation from R6/2 mice similar to ours exhibited normal or even increased striatal real-time glutamate uptake (Parsons et al., 2016). In line with this, we observed normal glutamate uptake in the striatum but a slight decrease in the uptake of glutamate in the cortex (Figure 5). Although glutamate uptake deficiency in HD remains debated, our data suggest a more prominent role for glutamine release in the pathogenesis of HD. We and others have observed elevated glutamine levels in R6/2 brains (Table S5; Behrens et al., 2002; Tsang et al., 2006; Tkac et al., 2007; Zacharoff et al., 2012), which could either indicate that astrocytic glutamine synthesis is increased or that glutamine release is impaired. The latter is in line with reduced expression of SNAT3 (Figure 3; Figure S5), whereas the former

Table 1. Central Protein Candidates in the R6/2 Mouse Model

	Striatum			Cortex			Hippocampus			Midbrain		
	Gene	FC	p Value	Gene	FC	p Value	Gene	FC	p Value	Gene	FC	p Value
Top 25 Proteins with Decreased Expression	Serpina1e	−12.46	6.7E−04	Serpina3m	−18.38	1.05E−03	Serpina3k	−67.45	1.16E−03	Serpina3k	−27.80	8.12E−05
	Atp11b	−11.68	2.7E−02	Serpina1e	−13.58	8.43E−04	Serpina3m	−47.24	2.97E−04	Serpina3m	−23.19	1.68E−04
	Serpina3k	−11.13	5.4E−03	Serpina3k	−8.62	3.28E−03	Serpina1e	−17.14	8.24E−04	Serpina1e	−21.16	2.22E−05
	Myl4	−9.23	4.8E−05	Sdk2	−6.08	1.81E−02	Fkbp5	−6.07	1.14E−02	Prkcd	−5.86	4.57E−05
	Serpina3m	−8.22	1.5E−02	Tph2	−5.16	7.47E−05	Rem2	−5.58	1.04E−02	Gjb6	−5.80	1.04E−04
	Rasgrp2	−7.87	1.2E−04	Mug1	−4.35	7.51E−04	Hexa	−4.60	2.49E−02	Mug1	−4.77	1.37E−03
	Pde10a	−7.63	5.4E−06	Magi3	−4.33	2.18E−05	Kctd4	−4.40	2.38E−04	Slc4a4	−4.44	1.18E−02
	Mug1	−7.60	4.3E−03	Ttpal	−4.09	2.15E−02	Itpka	−4.32	7.68E−05	Grid1	−4.41	5.48E−03
	Rgs9	−7.14	3.3E−04	Rasgrp2	−3.87	6.84E−03	Ptpn5	−4.15	6.81E−04	Tph2	−3.87	9.71E−04
	Adora2a	−7.08	1.7E−03	Pde10a	−3.81	1.94E−03	Tanc1	−4.03	7.72E−04	Etnppl	−3.76	2.79E−03
	Rem2	−6.32	3.0E−05	Ppp1r1b	−3.72	6.22E−05	Prkcd	−4.03	1.18E−02	Ckm	−3.75	1.44E−02
	Rasd2	−5.71	6.6E−05	Camkk2	−3.52	2.94E−06	Rin1	−3.95	2.45E−05	Cdkl5	−3.32	1.71E−02
	Scn4b	−5.67	7.6E−05	Prkcd	−3.46	2.88E−04	Trmt112	−3.83	5.14E−02	Serpina1a	−3.07	5.10E−03
	Penk	−5.12	4.5E−04	Cplx3	−3.45	1.41E−03	Homer3	−3.77	2.05E−04	Pla2g7	−2.97	1.53E−02
	Arc	−5.04	1.0E−02	Kctd4	−3.45	1.70E−03	Ppp1r16a	−3.50	3.58E−03	Cryab	−2.77	3.77E−04
	Dcun1d2	−5.02	1.2E−02	Itpka	−3.43	1.25E−04	Rasgrp1	−3.45	1.73E−04	Slc18a2	−2.71	6.92E−03
	Prkcd	−4.76	5.2E−07	Nptx2	−3.38	1.58E−02	Sypl1	−3.31	4.70E−02	Lrrtm1	−2.60	1.96E−03
	Acy1	−4.57	3.9E−03	Kifc2	−3.33	4.76E−02	Wfs1	−3.31	1.49E−04	Ccdc136	−2.55	4.44E−03
	Kcnip2	−4.55	1.3E−02	Eif4e2	−3.20	1.73E−02	Wipf3	−3.27	1.35E−03	Serpinb1a	−2.46	3.67E−04
	Sec14l1	−4.35	1.2E−03	Pdlim1	−3.17	3.29E−02	Myh10	−3.26	1.61E−02	Syt6	−2.45	1.36E−03
	Cyp2s1	−4.31	2.9E−03	Myl4	−3.15	4.32E−03	Tmod1	−3.26	2.32E−04	Fdps	−2.38	3.02E−04
	Spata2l	−4.29	1.5E−04	Gfra2	−3.02	4.79E−02	Grin2a	−3.15	3.65E−05	Cyp2j9	−2.38	1.17E−05
	Chmp1a	−4.29	1.4E−02	Ankrd63	−2.95	1.91E−02	Clic6	−3.12	4.70E−02	Sparc	−2.31	7.75E−03
	Ace	−4.27	6.3E−02	Arc	−2.78	5.20E−02	Gabra5	−2.98	8.25E−04	Kcnj10	−2.30	3.83E−04
	Snrpc	−4.26	9.1E−03	Tpm3	−2.76	4.23E−02	Tph2	−2.95	5.15E−03	9030617O03Rik	−2.28	8.53E−03

(*Continued on next page*)

Table 1. ***Continued***

	Striatum			Cortex			Hippocampus			Midbrain		
	Gene	FC	p Value	Gene	FC	p Value	Gene	FC	p Value	Gene	FC	p Value
Top 25 Proteins with Increased Expression	Crot	11.14	6.65E−02	Chd2	46.24	1.59E−02	Hap1	4.00	4.21E−02	Wdr5	3.7	6.68E−06
	Myl6b	6.48	1.04E−01	Hist3h2ba	10.99	1.05E−01	Pcsk1n	2.23	1.52E−04	Hist1h3a	3.2	3.08E−03
	Mapt	5.91	1.63E−02	Gm9242	7.04	7.87E−02	Gprasp1	2.20	8.60E−03	Oprm1	2.8	1.30E−03
	Hap1	5.60	1.07E−03	Slit3	6.41	8.82E−02	Nova1	2.14	2.88E−02	Akap8l	2.7	1.88E−03
	Gprasp1	5.59	1.36E−03	Abca7	6.14	5.09E−03	Irgm1	2.04	1.39E−03	Mri1	2.6	2.29E−04
	Acp1	5.44	3.83E−02	Cnnm3	5.32	1.04E−02	Pmm2	1.96	1.16E−03	Acy3	2.6	4.57E−03
	Copz1	5.14	5.24E−02	Mapt	5.04	2.32E−02	Mri1	1.87	3.98E−03	Stat1	2.2	6.32E−05
	Ank2	4.79	1.80E−02	Glrx5	5.00	4.76E−02	Elavl3	1.84	1.11E−02	Ftl1	2.1	6.70E−04
	Ftl1	4.16	2.76E−02	Hap1	3.93	2.42E−02	Mblac2	1.84	6.48E−03	Pmm2	2.0	1.58E−04
	Ahi1	4.12	4.27E−03	Ankle2	3.55	9.27E−02	Gaa	1.81	2.02E−03	Cmpk2	2.0	1.26E−03
	Ralyl	3.73	2.28E−02	Ccdc25	3.41	8.18E−02	Qrsl1	1.81	1.29E−02	Irgm1	1.9	5.88E−04
	Amacr	3.69	1.93E−02	B2m	3.38	8.23E−02	Gm20498	1.76	1.30E−02	Isg15	1.9	4.55E−03
	Fam81a	3.55	4.13E−02	Eif4ebp2	3.37	5.15E−02	Gng4	1.73	3.06E−03	Flnb	1.9	5.92E−03
	Pds5a	3.25	1.96E−02	Syne2	3.30	3.62E−02	Fundc2	1.70	2.85E−03	Cbx5	1.8	6.30E−03
	Mri1	3.25	6.82E−06	Paf1	3.29	2.95E−03	Usp4	1.70	9.44E−03	Marcksl1	1.8	3.97E−04
	Kiaa1109	3.21	2.33E−02	Fubp3	3.10	6.18E−02	Cmpk2	1.70	9.96E−04	Sh3bgrl	1.7	7.80E−04
	Cttnbp2nl	3.14	2.33E−02	Cep290	3.09	8.31E−02	Ctsa	1.65	1.18E−03	Glo1	1.7	2.30E−03
	Dus3l	2.96	5.26E−03	Myo9a	2.94	1.92E−02	Cirbp	1.63	7.05E−03	Mycbp2	1.7	5.19E−04
	Sf3b6	2.94	6.00E−02	Crk	2.94	1.32E−02	Copz1	1.61	2.49E−03	Rpl37a	1.7	4.24E−03
	Rlbp1	2.94	5.82E−02	Nudt12	2.92	2.95E−03	Enpp6	1.60	8.29E−03	Vwa5a	1.6	1.61E−03
	Map3k4	2.86	4.82E−02	Mri1	2.85	8.19E−05	Ublcp1	1.60	2.37E−03	Psmd4	1.6	3.60E−03
	Macrod1	2.84	1.96E−05	Rwdd1	2.85	5.46E−03	Fbxo22	1.60	2.24E−04	Luc7l2	1.6	5.27E−04
	Elavl2	2.77	2.98E−03	Dcc	2.79	1.82E−02	Ralyl	1.59	2.11E−02	D3Ertd751e	1.6	1.90E−03
	Tstd3	2.77	7.92E−02	Gprasp1	2.77	1.38E−02	Scrn2	1.58	1.78E−02	Rnpep	1.6	9.68E−04
	Cnot2	2.76	2.31E−02	Rp2	2.70	6.36E−02	Ptprn	1.56	5.06E−03	M6pr	1.6	3.05E−03

The proteins with the largest differential expression for each brain regions are shown for proteins with both increased and decreased expression in R6/2 compared with WT mice. The expression difference is stated as log2 fold change (FC), and the associated p value is illustrated.

appears less likely since we and others have observed decreased expression of GS in R6/2 brains (Liévens et al., 2002; Boussicault et al., 2014; Tong et al., 2014). Furthermore, we did not observe reductions in glutamine labeling or levels after incubation with either [U-^{13}C]glutamate or [U-^{13}C]glutamine, indicating normal GS activity and glutamine uptake, respectively. Overall, these results point toward dysfunctional astrocytic glutamine release, which may, in turn, explain the reduced neuronal GABA labeling observed after [U-^{13}C]glutamate or [1,2-^{13}C]acetate incubation (Sonnewald et al., 1993; Figures 4 and 5), consistent with reduced cerebral GABA levels in HD patients (Spokes et al., 1980; Patassini et al., 2016). Under baseline conditions, we observed a trend toward reduced GABA levels in striatal slices of R6/2 mice (Table S5), which supports neurodegeneration in this region, and since striatal neurons from R6/2 mice are more vulnerable compared with WT mice, it could be argued that a fraction of these neurons would be more susceptible to stress during the preparation of brain slices and cause the observed reduced ^{13}C labeling in GABA (Table S6). However, the percentage of ^{13}C labeling is calculated in relation to the total amount of the respective metabolite (Walls et al., 2014), and since the total cellular GABA amounts were unchanged in the extracts of the incubated slices from R6/2 and WT mice, the reduced ^{13}C enrichment in GABA is most likely due to reduced synthesis rather than reduced viability of GABAergic neurons in brain slices from R6/2 mice. This is also consistent with previous work demonstrating that brain slices can remain metabolically viable for up to 12 hr under appropriate conditions (Rae, 2014). Second, it could be discussed whether the findings are a consequence of neuronal loss because we are looking at end-stage R6/2 mice. Here, the previous notion of ^{13}C labeling normalization also applies, and this is further substantiated by normal GABA labeling after 60 min of incubation with either [U-^{13}C]glucose, [U-^{13}C]βHB, and [U-^{13}C]glutamine, indicating viable brain slices, in contrast to incubation with [1,2^{13}C] acetate or [U-^{13}C]glutamate, displaying significant astrocytic impairments.

The suggestion that the astrocyte is the culprit in HD is in line with recent studies showing impaired neuronal metabolism when co-cultured with astrocytes expressing mutant HTT (Boussicault et al., 2014), whereas metabolism is not noticeably affected in neurons from HD mouse models cultured alone (Boussicault et al., 2014; Hamilton et al., 2015, 2016). Furthermore, it has been shown that transplanted human astrocytes expressing mutant HTT can induce a HD pathology-like state in healthy mice, whereas transplanted healthy astrocytes can alleviate HD symptoms in R6/2 mice (Benraiss et al., 2016).

Our results indicate that metabolic defects are more prominent in astrocytes compared with neurons in the R6/2 brain and may take place as early as 8 weeks of age (Figure S5). However, since we used end-stage R6/2 mice for this study, we cannot conclude with certainty whether the astrocytic metabolic dysfunctions are part of the cause or a consequence of disease progression. Hence, functional metabolic follow-up studies at pre-symptomatic and early stages of the disease are desired to assess how early astrocytic metabolism is affected in R6/2 mice. In addition, validation of our findings in full-length HTT transgenic or knockin mouse models of HD, which display slower disease progression, would be of high scientific value and interest.

Collectively, our study shows that proteomics and ^{13}C mapping in combination are powerful tools to dissect metabolic pathways. Our data suggest that astrocytes could be a central driver behind HD pathology as result of impaired metabolism and glutamine release, leading to diminished neuronal GABA synthesis. This would lead to impaired inhibitory neurotransmission and, in turn, enhance the detrimental excitatory neurotransmission observed in HD. Hence, our data suggest that normalizing astrocyte metabolism may be a beneficial approach to restore or improve neuronal function in HD.

EXPERIMENTAL PROCEDURES

Further details and an outline of resources used in this work can be found in the Supplemental Experimental Procedures.

Mouse Strains

R6/2, transgenic for exon 1 of the human *HTT* gene (Mangiarini et al., 1996), originated from The Jackson Laboratory (Bar Harbor, Maine, USA) and were maintained by backcrossing males to CBA/j × B6 females (Taconic, Denmark). The mice were kept under specific pathogen-free conditions at a 12 hr light/12 hr darkness cycle in standard polystyrene cages with *ad libitum* access to standard chow and water. DNA was extracted from ear punches and used for genotyping (Andrew et al., 1994). The repeat length was between 190–200 CAG throughout the experiment. 12-week-old male mice were used for both proteomic and metabolic analysis. WT littermates without the *HTT* transgene were used as controls.

Statistical Analysis

The statistical tests are annotated in the figure legends and/or in the Supplemental Experimental Procedures for the specific analysis. The mean, SD, SEM, and significance levels are reported in the tables, figures, and/or in the legends. Statistical analyses for proteome data were performed using Perseus as described in the Supplemental Experimental Procedures for each individual analysis. Statistical analyses for brain slice incubation data were done in Prism 7, and the results are presented as means ± SEM. Outliers were identified using Grubb's outlier test ($\alpha = 0.05$). Statistical differences were tested using Student's unpaired t test, with a significance level of $p < 0.05$ indicated by a single asterisk. The exact p values can also be found in Tables S5 and S6.

Ethical Approval

Experiments were performed in accordance with the Danish Animal Experiments Inspectorate's guidelines (permit 2007/561-1345), the Danish Working Environment Authority (permit 20070033239/4), and European Commission Directive 86/609/EEC for animal experiments.

DATA AND SOFTWARE AVAILABILITY

The accession number for the MS-based proteomics data reported in this paper is ProteomeXchange Consortium: PXD008099.

SUPPLEMENTAL INFORMATION

Supplemental Information includes Supplemental Experimental Procedures, six figures, and six tables and can be found with this article online at https://doi.org/10.1016/j.celrep.2018.04.052.

ACKNOWLEDGMENTS

The work carried out in this study was in part supported by the Novo Nordisk Foundation Center for Protein Research, Novo Nordisk Foundation (grant agreement numbers NNF14CC0001 and NNF13OC0006477), Danish Council

for Independent Research grant agreements DFF 4002-00051 (*Sapere Aude*) and DFF 4183-00322A. The research was further supported by Stadslæge Svend Ahrend Larsen og Grosserer Jon Johannesons Fond. The Scholarship of Peter & Emma Thomsen is acknowledged for financial support to J.V.A. We thank the Department of Experimental Medicine and especially Bente Langelund Kristensen for help with R6/2 mouse breeding and caretaking and Rabab Nima for genotyping. We thank members of the NNF-CPR Mass Spectrometry Platform for instrument support and technical assistance.

AUTHOR CONTRIBUTIONS

N.H.S. performed mouse dissections and sample preparation and conducted LC-MS/MS experiments and data analysis. J.V.A. prepared brain slices, performed acute metabolic slice incubations, and conducted GC-MS experiments and data analysis. HPLC analysis was done by B.I.A. A.S. performed the network analysis. C.W.W. performed the clasping phenotyping of the mice. N.H.S., J.V.A., H.S.W., and M.L.N. interpreted the data. A.N. provided mice and reagents and helped with phenotyping analysis and results. N.H.S. and M.L.N. conceived the project, and N.H.S., J.V.A., and M.L.N. wrote the manuscript. All authors read and approved the manuscript.

DECLARATION OF INTERESTS

The authors declare no competing interests.

Received: November 17, 2017
Revised: February 23, 2018
Accepted: April 12, 2018
Published: May 15, 2018

REFERENCES

Achanta, L.B., Rowlands, B.D., Thomas, D.S., Housley, G.D., and Rae, C.D. (2017). β-Hydroxybutyrate Boosts Mitochondrial and Neuronal Metabolism but is not Preferred Over Glucose Under Activated Conditions. Neurochem. Res. *42*, 1710–1723.

Acuña, A.I., Esparza, M., Kramm, C., Beltrán, F.A., Parra, A.V., Cepeda, C., Toro, C.A., Vidal, R.L., Hetz, C., Concha, I.I., et al. (2013). A failure in energy metabolism and antioxidant uptake precede symptoms of Huntington's disease in mice. Nat. Commun. *4*, 2917.

Albrecht, J., and Schousboe, A. (2005). Taurine interaction with neurotransmitter receptors in the CNS: an update. Neurochem. Res. *30*, 1615–1621.

Albrecht, J., Sidoryk-Węgrzynowicz, M., Zielińska, M., and Aschner, M. (2010). Roles of glutamine in neurotransmission. Neuron Glia Biol. *6*, 263–276.

Andersen, J.V., Christensen, S.K., Aldana, B.I., Nissen, J.D., Tanila, H., and Waagepetersen, H.S. (2017a). Alterations in Cerebral Cortical Glucose and Glutamine Metabolism Precedes Amyloid Plaques in the APPswe/PSEN1dE9 Mouse Model of Alzheimer's Disease. Neurochem. Res. *42*, 1589–1598.

Andersen, J.V., McNair, L.F., Schousboe, A., and Waagepetersen, H.S. (2017b). Specificity of exogenous acetate and glutamate as astrocyte substrates examined in acute brain slices from female mice using methionine sulfoximine (MSO) to inhibit glutamine synthesis. J. Neurosci. Res. *95*, 2207–2216.

Andrew, S.E., Goldberg, Y.P., Theilmann, J., Zeisler, J., and Hayden, M.R. (1994). A CCG repeat polymorphism adjacent to the CAG repeat in the Huntington disease gene: implications for diagnostic accuracy and predictive testing. Hum. Mol. Genet. *3*, 65–67.

Attwell, D., and Laughlin, S.B. (2001). An energy budget for signaling in the grey matter of the brain. J. Cereb. Blood Flow Metab. *21*, 1133–1145.

Aylward, E.H., Nopoulos, P.C., Ross, C.A., Langbehn, D.R., Pierson, R.K., Mills, J.A., Johnson, H.J., Magnotta, V.A., Juhl, A.R., and Paulsen, J.S.; PREDICT-HD Investigators and Coordinators of Huntington Study Group (2011). Longitudinal change in regional brain volumes in prodromal Huntington disease. J. Neurol. Neurosurg. Psychiatry *82*, 405–410.

Aylward, E.H., Liu, D., Nopoulos, P.C., Ross, C.A., Pierson, R.K., Mills, J.A., Long, J.D., and Paulsen, J.S.; PREDICT-HD Investigators and Coordinators of the Huntington Study Group (2012). Striatal volume contributes to the prediction of onset of Huntington disease in incident cases. Biol. Psychiatry *71*, 822–828.

Badar-Goffer, R.S., Bachelard, H.S., and Morris, P.G. (1990). Cerebral metabolism of acetate and glucose studied by 13C-n.m.r. spectroscopy. A technique for investigating metabolic compartmentation in the brain. Biochem. J. *266*, 133–139.

Bak, L.K., Schousboe, A., Sonnewald, U., and Waagepetersen, H.S. (2006a). Glucose is necessary to maintain neurotransmitter homeostasis during synaptic activity in cultured glutamatergic neurons. J. Cereb. Blood Flow Metab. *26*, 1285–1297.

Bak, L.K., Schousboe, A., and Waagepetersen, H.S. (2006b). The glutamate/GABA-glutamine cycle: aspects of transport, neurotransmitter homeostasis and ammonia transfer. J. Neurochem. *98*, 641–653.

Bates, G.P., Dorsey, R., Gusella, J.F., Hayden, M.R., Kay, C., Leavitt, B.R., Nance, M., Ross, C.A., Scahill, R.I., Wetzel, R., et al. (2015). Huntington disease. Nat. Rev. Dis. Primers *1*, 15005.

Beal, M.F., Brouillet, E., Jenkins, B.G., Ferrante, R.J., Kowall, N.W., Miller, J.M., Storey, E., Srivastava, R., Rosen, B.R., and Hyman, B.T. (1993). Neurochemical and histologic characterization of striatal excitotoxic lesions produced by the mitochondrial toxin 3-nitropropionic acid. J. Neurosci. *13*, 4181–4192.

Behrens, P.F., Franz, P., Woodman, B., Lindenberg, K.S., and Landwehrmeyer, G.B. (2002). Impaired glutamate transport and glutamate-glutamine cycling: downstream effects of the Huntington mutation. Brain *125*, 1908–1922.

Bélanger, M., Allaman, I., and Magistretti, P.J. (2011). Brain energy metabolism: focus on astrocyte-neuron metabolic cooperation. Cell Metab. *14*, 724–738.

Benchoua, A., Trioulier, Y., Zala, D., Gaillard, M.-C., Lefort, N., Dufour, N., Saudou, F., Elalouf, J.-M., Hirsch, E., Hantraye, P., et al. (2006). Involvement of mitochondrial complex II defects in neuronal death produced by N-terminus fragment of mutated huntingtin. Mol. Biol. Cell *17*, 1652–1663.

Benraiss, A., Wang, S., Herrlinger, S., Li, X., Chandler-Militello, D., Mauceri, J., Burm, H.B., Toner, M., Osipovitch, M., Jim Xu, Q., et al. (2016). Human glia can both induce and rescue aspects of disease phenotype in Huntington disease. Nat. Commun. *7*, 11758.

Boussicault, L., Hérard, A.-S., Calingasan, N., Petit, F., Malgorn, C., Merienne, N., Jan, C., Gaillard, M.-C., Lerchundi, R., Barros, L.F., et al. (2014). Impaired brain energy metabolism in the BACHD mouse model of Huntington's disease: critical role of astrocyte-neuron interactions. J. Cereb. Blood Flow Metab. *34*, 1500–1510.

Brouillet, E., Hantraye, P., Ferrante, R.J., Dolan, R., Leroy-Willig, A., Kowall, N.W., and Beal, M.F. (1995). Chronic mitochondrial energy impairment produces selective striatal degeneration and abnormal choreiform movements in primates. Proc. Natl. Acad. Sci. USA *92*, 7105–7109.

Browne, S.E., and Beal, M.F. (2004). The energetics of Huntington's disease. Neurochem. Res. *29*, 531–546.

Camandola, S., and Mattson, M.P. (2017). Brain metabolism in health, aging, and neurodegeneration. EMBO J. *36*, 1474–1492.

Cong, W.-N., Cai, H., Wang, R., Daimon, C.M., Maudsley, S., Raber, K., Canneva, F., von Hörsten, S., and Martin, B. (2012). Altered hypothalamic protein expression in a rat model of Huntington's disease. PLoS ONE *7*, e47240.

Cummings, D.M., Alaghband, Y., Hickey, M.A., Joshi, P.R., Hong, S.C., Zhu, C., Ando, T.K., André, V.M., Cepeda, C., Watson, J.B., and Levine, M.S. (2012). A critical window of CAG repeat-length correlates with phenotype severity in the R6/2 mouse model of Huntington's disease. J. Neurophysiol. *107*, 677–691.

Deschepper, M., Hoogendoorn, B., Brooks, S., Dunnett, S.B., and Jones, L. (2012). Proteomic changes in the brains of Huntington's disease mouse

models reflect pathology and implicate mitochondrial changes. Brain Res. Bull. *88*, 210–222.

Díaz-García, C.M., Mongeon, R., Lahmann, C., Koveal, D., Zucker, H., and Yellen, G. (2017). Neuronal Stimulation Triggers Neuronal Glycolysis and Not Lactate Uptake. Cell Metab. *26*, 361–374.e4.

Dvorzhak, A., Vagner, T., Kirmse, K., and Grantyn, R. (2016). Functional Indicators of Glutamate Transport in Single Striatal Astrocytes and the Influence of Kir4.1 in Normal and Huntington Mice. J. Neurosci. *36*, 4959–4975.

Estrada-Sánchez, A.M., Montiel, T., Segovia, J., and Massieu, L. (2009). Glutamate toxicity in the striatum of the R6/2 Huntington's disease transgenic mice is age-dependent and correlates with decreased levels of glutamate transporters. Neurobiol. Dis. *34*, 78–86.

Foos, T.M., and Wu, J.-Y. (2002). The role of taurine in the central nervous system and the modulation of intracellular calcium homeostasis. Neurochem. Res. *27*, 21–26.

Guo, Z., Rudow, G., Pletnikova, O., Codispoti, K.-E., Orr, B.A., Crain, B.J., Duan, W., Margolis, R.L., Rosenblatt, A., Ross, C.A., and Troncoso, J.C. (2012). Striatal neuronal loss correlates with clinical motor impairment in Huntington's disease. Mov. Disord. *27*, 1379–1386.

Hamilton, J., Pellman, J.J., Brustovetsky, T., Harris, R.A., and Brustovetsky, N. (2015). Oxidative metabolism in YAC128 mouse model of Huntington's disease. Hum. Mol. Genet. *24*, 4862–4878.

Hamilton, J., Pellman, J.J., Brustovetsky, T., Harris, R.A., and Brustovetsky, N. (2016). Oxidative metabolism and Ca2+ handling in isolated brain mitochondria and striatal neurons from R6/2 mice, a model of Huntington's disease. Hum. Mol. Genet. *25*, 2762–2775.

Harris, J.J., Jolivet, R., and Attwell, D. (2012). Synaptic energy use and supply. Neuron *75*, 762–777.

Hosp, F., Gutiérrez-Ángel, S., Schaefer, M.H., Cox, J., Meissner, F., Hipp, M.S., Hartl, F.U., Klein, R., Dudanova, I., and Mann, M. (2017). Spatiotemporal Proteomic Profiling of Huntington's Disease Inclusions Reveals Widespread Loss of Protein Function. Cell Rep. *21*, 2291–2303.

Huang, K., Kang, M.H., Askew, C., Kang, R., Sanders, S.S., Wan, J., Davis, N.G., and Hayden, M.R. (2010). Palmitoylation and function of glial glutamate transporter-1 is reduced in the YAC128 mouse model of Huntington disease. Neurobiol. Dis. *40*, 207–215.

Khakh, B.S., Beaumont, V., Cachope, R., Munoz-Sanjuan, I., Goldman, S.A., and Grantyn, R. (2017). Unravelling and Exploiting Astrocyte Dysfunction in Huntington's Disease. Trends Neurosci. *40*, 422–437.

Kim, J., Moody, J.P., Edgerly, C.K., Bordiuk, O.L., Cormier, K., Smith, K., Beal, M.F., and Ferrante, R.J. (2010). Mitochondrial loss, dysfunction and altered dynamics in Huntington's disease. Hum. Mol. Genet. *19*, 3919–3935.

Leke, R., and Schousboe, A. (2016). The Glutamine Transporters and Their Role in the Glutamate/GABA-Glutamine Cycle. Adv. Neurobiol. *13*, 223–257.

Liévens, J.C., Woodman, B., Mahal, A., and Bates, G.P. (2002). Abnormal phosphorylation of synapsin I predicts a neuronal transmission impairment in the R6/2 Huntington's disease transgenic mice. Mol. Cell. Neurosci. *20*, 638–648.

Lim, R.G., Salazar, L.L., Wilton, D.K., King, A.R., Stocksdale, J.T., Sharifabad, D., Lau, A.L., Stevens, B., Reidling, J.C., Winokur, S.T., et al.; HD iPSC Consortium (2017). Developmental alterations in Huntington's disease neural cells and pharmacological rescue in cells and mice. Nat. Neurosci. *20*, 648–660.

Liu, X., Miller, B.R., Rebec, G.V., and Clemmer, D.E. (2007). Protein expression in the striatum and cortex regions of the brain for a mouse model of Huntington's disease. J. Proteome Res. *6*, 3134–3142.

Mangiarini, L., Sathasivam, K., Seller, M., Cozens, B., Harper, A., Hetherington, C., Lawton, M., Trottier, Y., Lehrach, H., Davies, S.W., and Bates, G.P. (1996). Exon 1 of the HD gene with an expanded CAG repeat is sufficient to cause a progressive neurological phenotype in transgenic mice. Cell *87*, 493–506.

McNair, L.F., Kornfelt, R., Walls, A.B., Andersen, J.V., Aldana, B.I., Nissen, J.D., Schousboe, A., and Waagepetersen, H.S. (2017). Metabolic Characterization of Acutely Isolated Hippocampal and Cerebral Cortical Slices Using [U-^{13}C]Glucose and [1,2-^{13}C]Acetate as Substrates. Neurochem. Res. *42*, 810–826.

Menalled, L., and Brunner, D. (2014). Animal models of Huntington's disease for translation to the clinic: best practices. Mov. Disord. *29*, 1375–1390.

Menzie, J., Pan, C., Prentice, H., and Wu, J.-Y. (2014). Taurine and central nervous system disorders. Amino Acids *46*, 31–46.

Mergenthaler, P., Lindauer, U., Dienel, G.A., and Meisel, A. (2013). Sugar for the brain: the role of glucose in physiological and pathological brain function. Trends Neurosci. *36*, 587–597.

Mochel, F., Durant, B., Meng, X., O'Callaghan, J., Yu, H., Brouillet, E., Wheeler, V.C., Humbert, S., Schiffmann, R., and Durr, A. (2012). Early alterations of brain cellular energy homeostasis in Huntington disease models. J. Biol. Chem. *287*, 1361–1370.

Naseri, N.N., Xu, H., Bonica, J., Vonsattel, J.P.G., Cortes, E.P., Park, L.C., Arjomand, J., and Gibson, G.E. (2015). Abnormalities in the tricarboxylic Acid cycle in Huntington disease and in a Huntington disease mouse model. J. Neuropathol. Exp. Neurol. *74*, 527–537.

Novak, M.J.U., and Tabrizi, S.J. (2010). Huntington's disease. BMJ *340*, c3109.

Parsons, M.P., Vanni, M.P., Woodard, C.L., Kang, R., Murphy, T.H., and Raymond, L.A. (2016). Real-time imaging of glutamate clearance reveals normal striatal uptake in Huntington disease mouse models. Nat. Commun. *7*, 11251.

Patassini, S., Begley, P., Xu, J., Church, S.J., Reid, S.J., Kim, E.H., Curtis, M.A., Dragunow, M., Waldvogel, H.J., Snell, R.G., et al. (2016). Metabolite mapping reveals severe widespread perturbation of multiple metabolic processes in Huntington's disease human brain. Biochim. Biophys. Acta *1862*, 1650–1662.

Perluigi, M., Poon, H.F., Maragos, W., Pierce, W.M., Klein, J.B., Calabrese, V., Cini, C., De Marco, C., and Butterfield, D.A. (2005). Proteomic analysis of protein expression and oxidative modification in r6/2 transgenic mice: a model of Huntington disease. Mol. Cell. Proteomics *4*, 1849–1861.

Rae, C. (2014). A Chip Off the Old Block: The Brain Slice as a Model for Metabolic Studies of Brain Compartmentation and Neuropharmacology (New York, NY: Springer New York), pp. 217–241.

Reynolds, R.H., Petersen, M.H., Willert, C.W., Heinrich, M., Nymann, N., Dall, M., Treebak, J.T., Björkqvist, M., Silahtaroglu, A., Hasholt, L., and Nørremølle, A. (2017). Perturbations in the p53/miR-34a/SIRT1 pathway in the R6/2 Huntington's disease model. Mol. Cell Neurosci. *88*, 118–129.

Rodrigues, F.B., Byrne, L.M., McColgan, P., Robertson, N., Tabrizi, S.J., Zetterberg, H., and Wild, E.J. (2016). Cerebrospinal Fluid Inflammatory Biomarkers Reflect Clinical Severity in Huntington's Disease. PLoS ONE *11*, e0163479.

Rosas, H.D., Salat, D.H., Lee, S.Y., Zaleta, A.K., Hevelone, N., and Hersch, S.M. (2008). Complexity and heterogeneity: what drives the ever-changing brain in Huntington's disease? Ann. N Y Acad. Sci. *1147*, 196–205.

Ross, C.A., and Tabrizi, S.J. (2011). Huntington's disease: from molecular pathogenesis to clinical treatment. Lancet Neurol. *10*, 83–98.

Sharma, K., Schmitt, S., Bergner, C.G., Tyanova, S., Kannaiyan, N., Manrique-Hoyos, N., Kongi, K., Cantuti, L., Hanisch, U.-K., Philips, M.-A., et al. (2015). Cell type- and brain region-resolved mouse brain proteome. Nat. Neurosci. *18*, 1819–1831.

Skotte, N.H., Sanders, S.S., Singaraja, R.R., Ehrnhoefer, D.E., Vaid, K., Qiu, X., Kannan, S., Verma, C., and Hayden, M.R. (2017). Palmitoylation of caspase-6 by HIP14 regulates its activation. Cell Death Differ. *24*, 433–444.

Sonnewald, U., Westergaard, N., Schousboe, A., Svendsen, J.S., Unsgård, G., and Petersen, S.B. (1993). Direct demonstration by [13C]NMR spectroscopy that glutamine from astrocytes is a precursor for GABA synthesis in neurons. Neurochem. Int. *22*, 19–29.

Spokes, E.G., Garrett, N.J., Rossor, M.N., and Iversen, L.L. (1980). Distribution of GABA in post-mortem brain tissue from control, psychotic and Huntington's chorea subjects. J. Neurol. Sci. *48*, 303–313.

Tadros, M.G., Khalifa, A.E., Abdel-Naim, A.B., and Arafa, H.M.M. (2005). Neuroprotective effect of taurine in 3-nitropropionic acid-induced experimental

animal model of Huntington's disease phenotype. Pharmacol. Biochem. Behav. *82*, 574–582.

Tang, B., Seredenina, T., Coppola, G., Kuhn, A., Geschwind, D.H., Luthi-Carter, R., and Thomas, E.A. (2011). Gene expression profiling of R6/2 transgenic mice with different CAG repeat lengths reveals genes associated with disease onset and progression in Huntington's disease. Neurobiol. Dis. *42*, 459–467.

Tang, C.C., Feigin, A., Ma, Y., Habeck, C., Paulsen, J.S., Leenders, K.L., Teune, L.K., van Oostrom, J.C.H., Guttman, M., Dhawan, V., and Eidelberg, D. (2013). Metabolic network as a progression biomarker of premanifest Huntington's disease. J. Clin. Invest. *123*, 4076–4088.

Tkac, I., Dubinsky, J.M., Keene, C.D., Gruetter, R., and Low, W.C. (2007). Neurochemical changes in Huntington R6/2 mouse striatum detected by in vivo 1H NMR spectroscopy. J. Neurochem. *100*, 1397–1406.

Todd, A.C., Marx, M.-C., Hulme, S.R., Bröer, S., and Billups, B. (2017). SNAT3-mediated glutamine transport in perisynaptic astrocytes in situ is regulated by intracellular sodium. Glia *65*, 900–916.

Tong, X., Ao, Y., Faas, G.C., Nwaobi, S.E., Xu, J., Haustein, M.D., Anderson, M.A., Mody, I., Olsen, M.L., Sofroniew, M.V., and Khakh, B.S. (2014). Astrocyte Kir4.1 ion channel deficits contribute to neuronal dysfunction in Huntington's disease model mice. Nat. Neurosci. *17*, 694–703.

Tsang, T.M., Woodman, B., McLoughlin, G.A., Griffin, J.L., Tabrizi, S.J., Bates, G.P., and Holmes, E. (2006). Metabolic characterization of the R6/2 transgenic mouse model of Huntington's disease by high-resolution MAS 1H NMR spectroscopy. J. Proteome Res. *5*, 483–492.

Waldvogel, H.J., Kim, E.H., Tippett, L.J., Vonsattel, J.P., and Faull, R.L. (2015). The Neuropathology of Huntington's Disease. Curr. Top. Behav. Neurosci. *22*, 33–80.

Walls, A.B., Bak, L.K., Sonnewald, U., Schousboe, A., and Waagepetersen, H.S. (2014). Metabolic Mapping of Astrocytes and Neurons in Culture Using Stable Isotopes and Gas Chromatography-Mass Spectrometry (GC-MS). In Brain Energy Metabolism, H.S. Waagepetersen and H. J, eds. (Humana Press), pp. 73–105.

Walls, A.B., Waagepetersen, H.S., Bak, L.K., Schousboe, A., and Sonnewald, U. (2015). The glutamine-glutamate/GABA cycle: function, regional differences in glutamate and GABA production and effects of interference with GABA metabolism. Neurochem. Res. *40*, 402–409.

Wegrzynowicz, M., Holt, H.K., Friedman, D.B., and Bowman, A.B. (2012). Changes in the striatal proteome of YAC128Q mice exhibit gene-environment interactions between mutant huntingtin and manganese. J. Proteome Res. *11*, 1118–1132.

Wilson, H., Niccolini, F., Haider, S., Marques, T.R., Pagano, G., Coello, C., Natesan, S., Kapur, S., Rabiner, E.A., Gunn, R.N., et al. (2016). Loss of extra-striatal phosphodiesterase 10A expression in early premanifest Huntington's disease gene carriers. J. Neurol. Sci. *368*, 243–248.

Wu, L.L.-Y., and Zhou, X.-F. (2009). Huntingtin associated protein 1 and its functions. Cell Adhes. Migr. *3*, 71–76.

Zabel, C., Chamrad, D.C., Priller, J., Woodman, B., Meyer, H.E., Bates, G.P., and Klose, J. (2002). Alterations in the mouse and human proteome caused by Huntington's disease. Mol. Cell. Proteomics *1*, 366–375.

Zabel, C., Mao, L., Woodman, B., Rohe, M., Wacker, M.A., Kläre, Y., Koppelstätter, A., Nebrich, G., Klein, O., Grams, S., et al. (2009). A large number of protein expression changes occur early in life and precede phenotype onset in a mouse model for Huntington disease. Mol. Cell. Proteomics *8*, 720–734.

Zacharoff, L., Tkac, I., Song, Q., Tang, C., Bolan, P.J., Mangia, S., Henry, P.-G., Li, T., and Dubinsky, J.M. (2012). Cortical metabolites as biomarkers in the R6/2 model of Huntington's disease. J. Cereb. Blood Flow Metab. *32*, 502–514.

Zuccato, C., Valenza, M., and Cattaneo, E. (2010). Molecular mechanisms and potential therapeutical targets in Huntington's disease. Physiol. Rev. *90*, 905–981.